Received February 28, 2019, accepted March 24, 2019, date of publication April 2, 2019, date of current version April 19, 2019.

Digital Object Identifier 10.1109/ACCESS.2019.2908411

Steady Flow Force Compensation and Test Research on Electrohydraulic Proportional Relief Valve

DAOHAI QU[1,2], YUNSHAN ZHOU[1,2], YUNFENG LIU[1], WEI LUO[1,2], AND FEITIE ZHANG[1]

[1]State Key Laboratory of Advanced Design and Manufacturing for Vehicle Body, Hunan University, Changsha 410012, China
[2]Hunan Rongda Vehicle Transmission Co., Ltd., Changsha 410205, China

Corresponding author: Feitie Zhang (flyiron@126.com)

This work was supported by the National Natural Science Foundation of China under Grant 51475151.

ABSTRACT The pressure control accuracy of electrohydraulic proportional relief valve (EPRV) is affected by steady flow force. Thus, this paper investigates the method of designing a spool groove into the turbine bucket profile to compensate for the steady flow force maximally. The influence of steady flow force on the working pressure of the EPRV is analyzed. The calculation model of the steady flow force is deduced. Moreover, the computational fluid dynamics (CFD) model of the spool is established considering the fitting clearance between the spool and the valve body. The test bench is built to verify the CFD model. The turbine bucket profile is designed in the spool groove and optimized on the basis of the response surface method. Furthermore, the flow impact coefficient is defined and the compensation effect of the optimized spool to the steady flow force is tested. The results show that the absolute error value of the CFD simulation and test is smaller than 6.51%. When the working pressure is 0.5, 2, and 4 MPa, the flow impact coefficients of the optimized spool can be reduced by 100%, 59.15%, and 26.72%, respectively, compared with the original spool, indicating that the optimized spool can obviously compensate the steady flow force and improve the control accuracy of the EPRV.

INDEX TERMS Electrohydraulic proportional relief valve (EPRV), steady flow force, turbine bucket profile, fitting clearance, response surface method (RSM), flow impact coefficient.

NOMENCLATURE

F_{pilot}	force from pilot chamber pressure (N)
F_{spring}	force from compressed spring (N)
F_{feedback}	force from feedback chamber pressure (N)
F_{s}	steady flow force (N)
p_{pilot}	pressure in pilot chamber (MPa)
p_1	pressures in main chamber (MPa)
A_{pilot}	effective area of pilot pressure (m^2)
A_{feedback}	effective area of feedback pressure (m^2)
k	spring stiffness (N/m)
x	compression length of spring (m)
Δx	throttle opening (m)
Δr	fitting clearance (m)
q	flow running through the groove (L/min)
p_2	pressures in overflow chamber (MPa)
d	outside diameter of spool (m)
D	inner diameter of valve body (m)
F_{rod}	viscous frictional force (N)
F_{dynamics}	force caused by dynamic pressure (N)
F_{statics}	force caused by static pressure (N)
p_{rs}	static pressure acted on right groove annular (MPa)
p_{ls}	static pressure acted on left groove annular (MPa)
p_{rd}	dynamic pressure acted on right groove annular (MPa)
p_{ld}	dynamic pressure acted on left groove annular (MPa)
A_{r}	right annular area of spool groove (m^2)
A_{l}	left annular area of spool groove (m^2)
A_{rod}	surface area of valve stem (m^2)
τ_{rod}	shear stress acted on valve stem by fluid (MPa)
F_{sleeve}	force of valve body that acts on fluid (N)
τ_{sleeve}	shear stress acts on fluid by valve body (MPa)
A_{sleeve}	contacting surface between valve body and control fluid (m^2)

The associate editor coordinating the review of this manuscript and approving it for publication was Huaqing Li.

α	geometric shape coefficient of the spool groove
μ	fluid viscosity (kg/m·s)
L	axial length between center from inlet to outlet (m)
ρ	fluid density (kg/m^3)
$\boldsymbol{v}$	fluid velocity (m/s)
v_x	axial fluid velocity (m/s)
A_{inlet}	surface that fluid flows in the spool groove (m^2)
A_{outlet}	surface that fluid flows out the spool groove (m^2)
R	radius of the arc groove(m)
θ	conical angle (°)
H	conical height (m)
CFD	computational fluid dynamics
EPRV	electrohydraulic proportional relief valve
RSM	response surface method
CCD	central composed design

I. INTRODUCTION

Electrohydraulic proportional control technology is used extensively in the field of automatic control area. The pressure control accuracy of electrohydraulic proportional control valve must be extremely high to control the force of actuator precisely [1]–[3]. However, achieving high-pressure control accuracy in the electrohydraulic proportional control valve is difficult due to complex and changeable working environment. Taking the automatic transmission as an example, the pump is used to provide oil to actuators, such as the wet clutch, and the electrohydraulic proportional relief valve (EPRV), whose schematic diagram is shown in Fig. 1, is used to control the pump outlet pressure. Given that the pump is directly driven by the engine with a wide range of rotational speed, the pump flow into the hydraulic system extensively changes. On the basis of different driving requirements, driving conditions, and engine displacement, the output torque of engines often varies in a wide range, thereby resulting in the extensive change of pressure demand of EPRVs [4]. The steady flow force of the spool increases with the flow and pressure difference on both sides of the spool meter edge [5], [6], thereby changing the mechanical equilibrium of the spool and increasing the working pressure of the EPRV. It would generate more fuel consumption and shorten the service life of the pump [4]. Therefore, compensating the steady flow force of the EPRV is necessary.

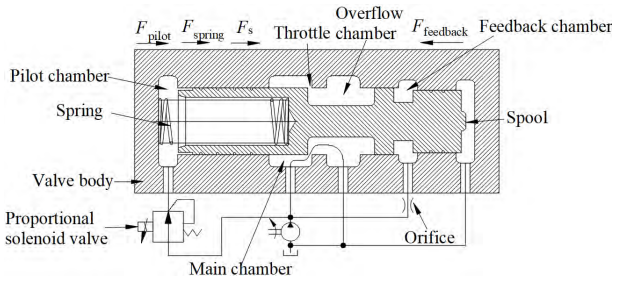

FIGURE 1. Structural diagram of EPRV.

Scholars have proposed several methods for compensating steady flow force. Xie *et al.* [7] designed a damping tail structure, which was optimized through the computational fluid dynamics (CFD) simulation, to compensate the steady flow force acting on the conical poppet. The test and simulation results showed that the design could compensate more than 80% of the flow force. Altare *et al.* [8] and Finesso and Rundo [9] compensated the flow force of cone relief valve through optimizing the shape of the diversion plate and the conical angle. The above steady flow force compensation methods are only suitable for electrohydraulic proportional control conical valve, but not suitable for electrohydraulic proportional control sliding valve. Blackburn *et al.* [10] and Merritt *et al.* [11].

proposed to design a turbine bucket profile in the groove of meter-in spool to compensate steady flow force. On this basis, Lugowski [12] proposed that the steady flow force compensation of turbine bucket profile is caused by the high inlet pressure that acts on the meter edge. Although the above scholars proposed that the turbine bucket profile could compensate steady flow force of spool, they had not studied on how to optimize the profile to compensate the flow force maximally. Borghi *et al.* [13] compensated the steady flow force of meter-in spool by designing a 45° cone at the groove outlet, and a round corner at the groove inlet and the valve body outlet respectively. Aung *et al.* [14] studied the manner in which a simple jet-guiding groove is dug at the annular side where the fluid flows out of the meter-out spool. The simulation results showed that this design could compensate 80% of the steady flow force, however, the authors did not verify the feasibility of the scheme by experiment. Simic and Herakovic [15] designed a conical surface at the position where the fluid flows in and out the groove, and optimized the conical angle and the throttle covering of spool to compensate the steady flow force. To compensate steady flow force of four-way three-position directly operated proportional directional valve, Amirante *et al.* [16]–[19] proposed to design a conical surface and throttle at the meter edge of the spool, and a conical surface in the spool groove where the fluid flows in. The steady flow force compensation methods developed by above scholars were only verified on high power electrohydraulic proportional sliding valves, the feasibility of low power electrohydraulic proportional control sliding valves had not been studied. And they used the traditional method to optimize the proposed steady flow force compensation structures, however, the optimal solution obtained by the traditional method can only be selected in a limited number of schemes, which means that it can not theoretically get the optimal solution.

As for the unfinished work and inadequacies of above scholars, this paper takes the low power EPRV as the research object, in which the spool is meter-in. The method of designing the turbine bucket profile in the spool groove to compensate steady flow force is verified. In order to obtain the optimal solution in theory, the shape parameters of the

turbine bucket profile are optimized by the response surface method (RSM).

First, the influence of steady flow force on the working pressure of the EPRV is analyzed, and the steady flow force calculation model is deduced. Second, the CFD model of the spool is established, considering the fitting clearance between the spool and the valve body, and the test platform is constructed to verify the model. Third, the turbine bucket profile is designed and parameterized in the spool groove and optimized by the RSM to compensate the steady flow force maximally. Finally, the effect of steady flow force compensation on the EPRV by the optimized spool is verified.

II. EFFECT OF STEADY FLOW FORCE ON EPRV

Fig. 1 shows the structural diagram of the pilot EPRV, which comprises a spool, spring, proportional solenoid valve, and valve body.

When the driving current of the proportional solenoid valve and the outlet flow of the pump remain unchanged, the throttle opening is assumed to slightly change. The inertias of spool, transient flow force, frictional force, and pressure drop loss of the orifice can be neglected. The spool will be affected by four forces, namely, F_{pilot}, F_{spring}, F_{feedback} and F_{s}. F_{pilot}, whose direction is to the right, is controlled by the pressure of proportional solenoid valve in the pilot chamber. F_{spring}, whose direction is to the right, is produced by the compressed spring. F_{feedback}, whose direction is to the left, is constructed by the flow running through the orifice in the feedback chamber. F_{s}, whose direction is to the right, is caused by the excess flow in the main chamber running through the overflow chamber through the throttle. When the total force of F_{pilot}, F_{spring} and F_{s} are larger than F_{feedback} and the velocity of the spool to the left direction is zero, the spool begins to move to the right direction and the throttle opening gradually decreases. Thus, the flow resistance of the throttle will become larger, the pressure in the feedback chamber will increases and F_{feedback} becomes larger. When F_{feedback} are larger than the total force of F_{pilot}, F_{spring} and F_{s} and the velocity of the spool to the right direction is zero, the spool begins to move to the left direction and the throttle opening gradually increases. Therefore, the flow resistance of the throttle will become smaller, the pressure in the feedback chamber will decreases and F_{feedback} becomes smaller. The EPRV maintains the pressure stability of the main chamber through its self-feedback regulation. The mechanical balance relationship of the spool is

$$\begin{aligned} F_{\text{pilot}} + F_{\text{s}} + F_{\text{spring}} &= F_{\text{feedback}}, \\ F_{\text{pilot}} &= p_{\text{pilot}} A_{\text{pilot}}, \\ F_{\text{feedback}} &= p_1 A_{\text{feedback}}, \\ F_{\text{spring}} &= kx, \end{aligned} \tag{1}$$

where p_{pilot} is the pressure of the pilot chamber, which is determined by the driving current of the proportional solenoid valve; p_1 is the pressure of the main chamber which is the working pressure of the EPRV; A_{pilot} and A_{feedback} are the effective pressure acting areas of the pilot and feedback chambers, respectively; k is the spring stiffness; and x is the compression length of the spring.

$$p_1 = \frac{p_{\text{pilot}} A_{\text{pilot}} + F_{\text{s}} + kx}{A_{\text{feedback}}}. \tag{2}$$

Given that A_{pilot}, A_{feedback}, k, and x are approximately constant when the driving current of the EPRV is unchanged, the working pressure in the main chamber of the EPRV will be affected by the steady flow force.

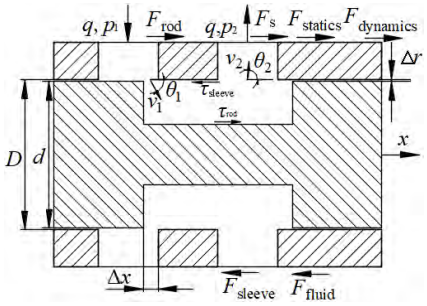

FIGURE 2. Throttling area of meter-in spool.

III. CALCULATION MODEL OF STEADY FLOW FORCE

Steady flow force, which is caused by the change in velocity when the fluid flows in and out of the spool groove, is the reaction force that acts on the axial direction of the spool. The essence of the steady flow force is the different forces caused by uneven pressure distribution on the annular sides of the groove, and the viscous frictional force acts on the spool when the fluid flows through the groove. Therefore, the region that produces the steady flow force is extracted for investigation, as shown in Fig. 2. From the figure, Δx is the throttle opening of the spool; Δr is the fitting clearance between the spool and the valve body; q is the flow running through the groove; p_1 and p_2 are the pressures of the main chamber flowing in with the fluid and the overflow chamber flowing out with the fluid, respectively; d is the outside diameter of the spool; and D is the inner diameter of the valve body.

Taking the spool as the research subject, the calculation model of F_{s} can be obtained as follows:

$$\begin{aligned} F_s &= F_{\text{rod}} + F_{\text{dynamics}} + F_{\text{statics}}, \\ F_{\text{rod}} &= \int\int_{A_{\text{rod}}} \tau_{\text{rod}} dA, \\ F_{\text{dynamics}} &= \int\int_{A_r} p_{\text{rd}} dA - \int\int_{A_{\text{l}}} p_{\text{ld}} dA, \\ F_{\text{statics}} &= \int\int_{A_{\text{r}}} p_{\text{rs}} dA - \int\int_{A_{\text{l}}} p_{\text{ls}} dA, \end{aligned} \tag{3}$$

where F_{rod} is the viscous frictional force applied to the spool stem due to fluid viscosity; F_{dynamics} is the dynamic force applied to the annular side of the groove for the fluid dynamic pressure; F_{statics} is the static force applied to the annular side of the groove for the fluid static pressure; p_{rs} and p_{ls} are the static pressures that act on the right and left annular sides of

the groove, respectively; p_{rd} and p_{ld} that act on the annular sides of the groove are the dynamic pressures caused by the transformation of the fluid kinetic energy into the pressure energy; A_r and A_l are the right and left annular side areas of the spool groove, respectively; A_{rod} is the surface area of the valve stem; and τ_{rod} is the shear stress applied on the valve stem by fluid.

Taking the control fluid of the spool groove as the research object, the resultant force F_{fluid} can be expressed as follows:

$$\begin{aligned} F_{fluid} &= -F_s + F_{sleeve}, \\ F_{sleeve} &= \iint_{A_{sleeve}} \tau_{sleeve} dA \approx \alpha \mu L q, \end{aligned} \tag{4}$$

where F_{sleeve} is the force of the valve body that acts on the fluid, τ_{sleeve} is the shear stress of the valve body that acts on the fluid, A_{sleeve} is the contacting surface between the valve body and the control fluid, α is the geometric shape coefficient of the spool groove [20], μ is the fluid viscosity, and L is the effective length of the fluid that moves along the axial direction in the spool groove.

As the direction of F_{fluid} is to the left in Fig. 2, the conservation of momentum yields the following:

$$\begin{aligned} F_{fluid} = \frac{d}{dt} \iiint_{C.V.} \rho v_x dV + \iint_{A_{inlet}} \rho v_x v \cdot i dA \\ + \iint_{A_{outlet}} \rho v_x v \cdot (-i)\, dA, \end{aligned} \tag{5}$$

where ρ is the fluid density; $\boldsymbol{v}$ and v_x are the velocity of fluid and its axial component along the spool's axial direction, respectively; A_{inlet} and A_{outlet} are the areas that the fluid flows in and out of the spool groove, respectively; and $\boldsymbol{i}$ is the left unit normal vector. The first term on the right side of Formula (5) is the transient flow force on the spool, and the second and third terms are the steady flow force. This study focuses on the force of the spool under a steady flow; thus, the influence of transient flow force on the spool is neglected.

By using v_1, v_2 and θ_1, θ_2 as the average velocities and the angles of fluid flowing in and out of the spool groove, respectively, Formula (5) can be simplified as follows:

$$F_{fluid} = \rho q v_1 \cos\theta_1 - \rho q v_2 \cos\theta_2. \tag{6}$$

Formulas (4) and (6) can yield the following:

$$F_s = \rho q v_1 \cos\theta_1 - \rho q v_2 \cos\theta_2 + \alpha \mu L q. \tag{7}$$

Therefore, the steady flow force that acts on the spool is related to the values of θ_1 and θ_2, and the steady flow force can be reduced by increasing θ_1 and decreasing θ_2.

IV. MODEL VERIFICATION

The fitting clearance between the spool and the valve body will be designed to ensure the smooth movement of the spool inside the valve body without stagnation due to machining accuracy, installation error, and impurity particles contained by the oil. Simultaneously, the designed fitting clearance should be reasonably controlled to reduce the leakage between the spool and the valve body [21]. The fitting clearance between the hydraulic relatively moving parts is generally designed between a few to dozens of microns [22]. However, most scholars have ignored the influence of the fitting clearance between the spool and the valve body when the spool CFD model is constructed to study the steady flow force of spool [23]–[25]. For illustrating the necessity of considering the fitting clearance between the spool and the valve body when building the spool CFD model, the fitting clearance of 20μm is selected as the validating object. The dimensional drawing (in mm) of the extracted spool calculation model is shown in Fig. 3. The spool model without considering fitting clearance is simulated by the spool model with 0μm fitting clearance. The two spool models with different fitting clearances are compared by numerical simulation and model verification respectively.

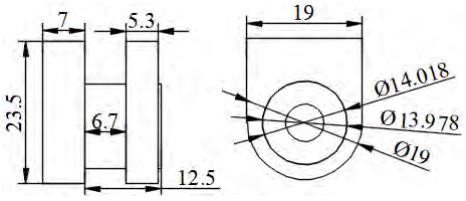

FIGURE 3. Dimensional drawing of spool model.

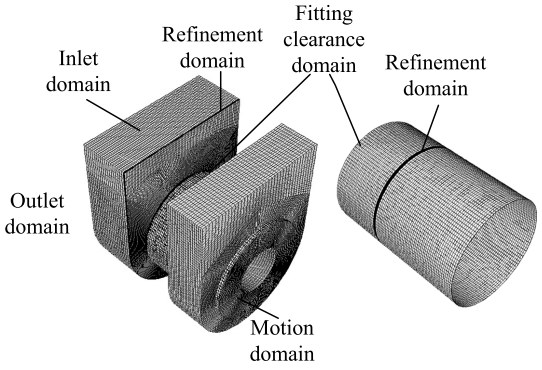

FIGURE 4. Computational domain grids of fluid.

A. NUMERICAL SIMULATION

The spool CFD model is divided into four domains, namely, inlet, fitting clearance, motion, and outlet domains, as shown in Fig. 4. First, the grids are divided by ICEM CFD software. Local refinement is conducted in the throttle area of the spool to reduce the computing time and ensure the accuracy of the spool CFD model, and grid independence is used to verify that the determined number of grids is approximately 1.4 million in total. Then, the divided grids are imported into Fluent software. As the sliding mesh has better convergence and applicability than the dynamic mesh in analytical process of three-dimensional transient parallel sliding flow field [26], this paper chooses the sliding mesh to simulate. The main setup steps of pre-processing in Fluent are as follows:

(1) Models: The standard k-ε model is selected as the viscous model.

(2) Materials: The density and the dynamic viscosity of the fluid are 847.7 kg/m^3 and 0.05 kg/m·s respectively.
(3) Boundary conditions: The inlet domain is set as the velocity inlet whose value is determined by the different inlet flows. The motion domain, which represents the fluid flowing through the spool groove, moves along the axial direction of the spool, and the speed is set to 2×10^{-6} m/s. The outlet domain is set as the pressure outlet whose value is 0.1 MPa. The contacting surfaces between different domains are set as the interface. The remaining surfaces are set as the stationary wall with no slip.
(4) Mesh interfaces: Two pairs of interfaces are set up, one of which is the contacting interface between the inlet, the outlet and the fitting clearance domains, the other of which is the contacting surface between the motion and the fitting clearance domains.
(5) Convergence criteria: The residual values of continuity, x-velocity, y-velocity, z-velocity, k and epsilon are less than 10^{-3}.
(6) Surface monitors: Formula (3) is used to calculate steady flow force of the motion domain.

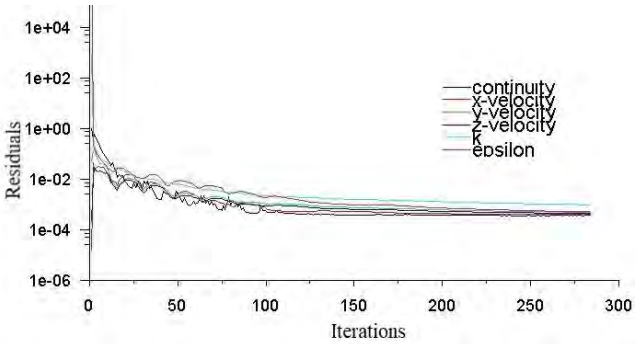

FIGURE 5. The convergence history of residuals with iterations.

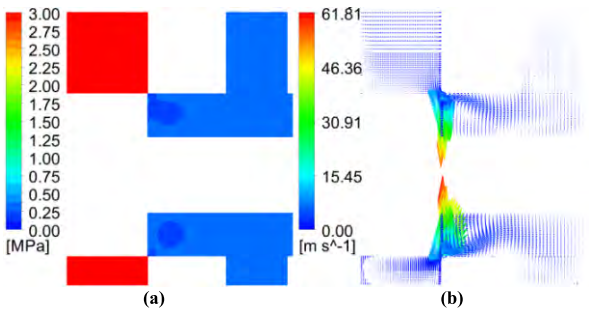

FIGURE 6. Simulation results when $\Delta r = 0$ μm. (a) Pressure cloud map. (b) Velocity vector map.

The spool CFD model converges when the iterations are closed to 282 as shown in Fig. 5.When the inlet flow is 12 L/min and the total pressure is 3 MPa, the pressure cloud and velocity vector cross-sectional maps with 0 μm and 20 μm fitting clearances are shown in Figs. 6 and 7, respectively. It can be clearly seen that the jet angle and the velocity value of the fluid flowing through the throttle in Fig. 7 are

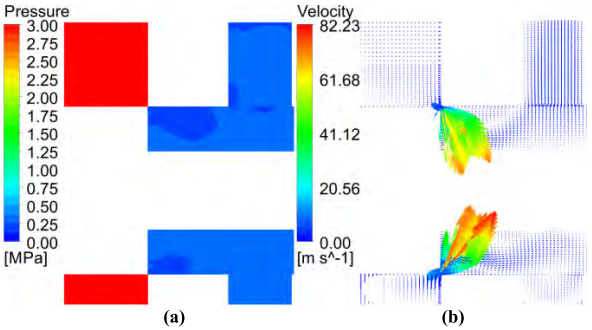

FIGURE 7. Simulation results when $\Delta r = 20$ μm. (a) Pressure cloud map. (b) Velocity vector map.

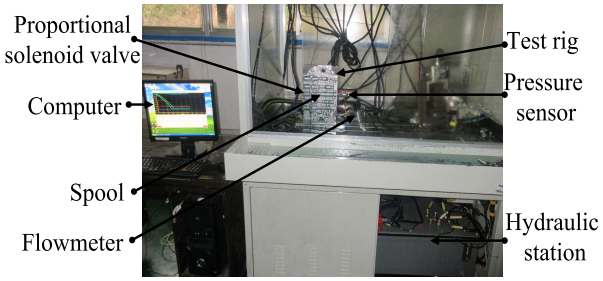

FIGURE 8. Test bench.

evidently difference from that in Fig. 6, It is mainly because the throttle opening of spool is very small while the low power EPRV works. When the fitting clearance is 0μm, the fluid in the inlet domain injects into the motion domain directly. The normal of flow surface is perpendicular to the axis of motion domain. When the fitting clearance is 20μm, the fluid in the inlet domain flows through the fitting clearance domain firstly before injecting into the motion domain, which would lead the normal of flow surface and the axis of motion domain form a sharp angle. The difference of flow surfaces would affect the jet angle of fluid, thus affecting the velocity of fluid. The Reynolds numbers at the throttle in Fig. 6 and Fig. 7 are 2483.6 and 2091.2, respectively. Therefore, the fitting clearance between the spool and the valve body affects the state variables(jet angle, velocity, Reynolds number, etc.) of the fluid in the spool groove to a large extent.

B. MODEL VERIFICATION

The test bench is constructed as shown in Fig. 8, and the hydraulic circuit of the test bench is shown in Fig. 9. The flowmeter selects the type of turbine and has the function of anti-electromagnetic interference and electronic digital display. The measuring range and accuracy of flowmeter are 3–20 L/min and 1%, respectively. The measuring range and accuracy of the pressure sensor are 0–6 MPa and 0.5%, respectively. The pump is a type of double-acting vane pump, and the single pump displacement is 7.5 mL/r. The motor speed range is 0–2400 r/min. The input current range and working pressure range of the proportional solenoid valve are 0–1 A and 0–0.6 MPa, respectively.

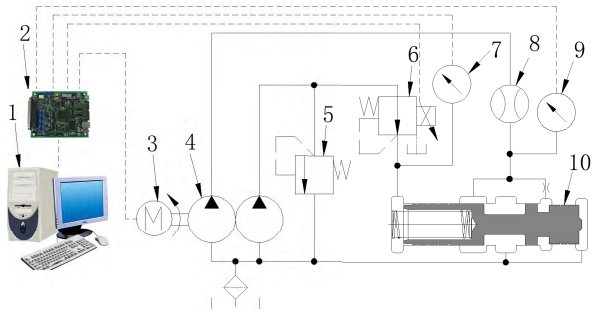

FIGURE 9. Hydraulic circuit of test bench. 1. Computer; 2. Control unit; 3. Driving motor; 4. Dual-acting vane pump; 5. Relief valve with constant pressure; 6. Proportional solenoid valve; 7, 9. Pressure sensors; 8. Flowmeter; 10. Spool.

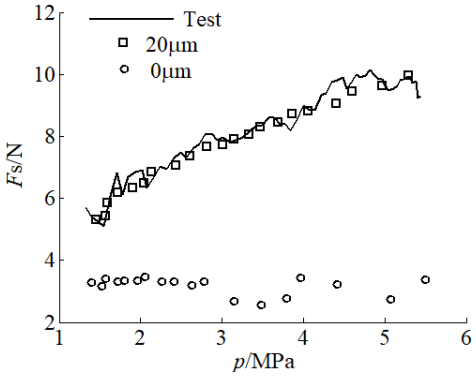

FIGURE 10. $q = 12$ L/min.

The driving current of the proportional solenoid valve is changed from 0 A to 1 A linearly, the current change interval is 0.001 A, and the change frequency is 50 Hz. The pressures of proportional solenoid valve p_{pilot} and spool main chamber p are measured by pressure sensors 7 and 9, respectively. The spool can be considered to work constantly near the throttle as the driving current changes slowly. That is to say, the influence of transient flow and frictional and inertial forces on the spool can be neglected. Given that the spring stiffness is relatively small, the spring can be considered to be constantly maintained in the pre-tightening force. Therefore, Formula (2) can be used to calculate the steady flow force of the spool under different working pressures.

When the overflow of the spool is 12 L/min and 18 L/min, the relationships between the steady flow force of the simulation values with fitting clearance of 0 μm and 20 μm and the main chamber pressure are compared with the those between the steady flow force of the test and the main chamber pressure, as shown in Figs. 10 and 11, respectively. The simulation results of the spool CFD model that considers the fitting clearance are evidently in good agreement with those in trend and numerical values under different overflow conditions. The steady flow force linearly increases with the pressure. And the absolute error value of the test and simulation is smaller than 6.51%. However, the simulation results without considering the fitting clearance are clearly different from the test data in trend and numerical values.

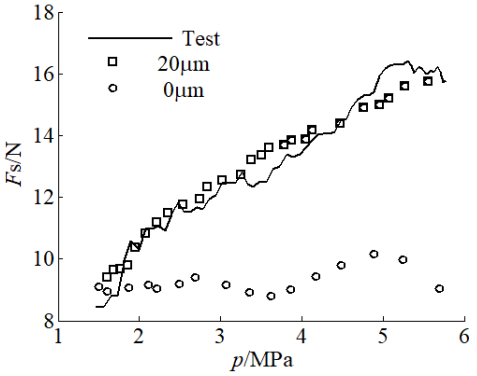

FIGURE 11. $q = 18$ L/min.

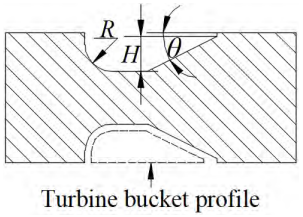

FIGURE 12. Turbine bucket profile.

Therefore, the CFD model that considers the fitting clearance can accurately calculate the steady flow force of the spool compared with that without considering the fitting clearance.

V. OPTIMAL DESIGN

In this study, the turbine bucket profile is designed in the spool groove to change the jet angle of the fluid flowing in and out of the groove; such a design essentially changes the pressure distribution on the annular side of the groove (Fig. 12). R, H, and θ represent the radius of the arc groove, the conical height, and the conical angle, respectively. The optimization of the profile parameters of the turbine bucket to compensate the steady flow force maximally has become an important research topic.

Optimal design methods mainly use the traditional approach and the RSM. The optimal solution obtained by the traditional method can only be selected in a limited number of schemes, which aid determine the accuracy of the optimization. The RSM is a collection of mathematical and statistical analysis techniques based on the fit of a polynomial equation to the experimental data, which must describe the behavior of a data set to provide statistical previsions. The objective is to optimize the levels of those variables simultaneously to attain the best system performance [27]–[29]. RSM is more suitable for optimization of multi-variable processes in a global design space of variables than the traditional method due to the limitation of time and economic conditions. Given that the turbine bucket profile is influenced by R, θ, and H, this study uses ANSYS Workbench software in designing and optimizing the profile parameters of the turbine bucket based on RSM. The optimization design flowchart is shown in Fig. 13.

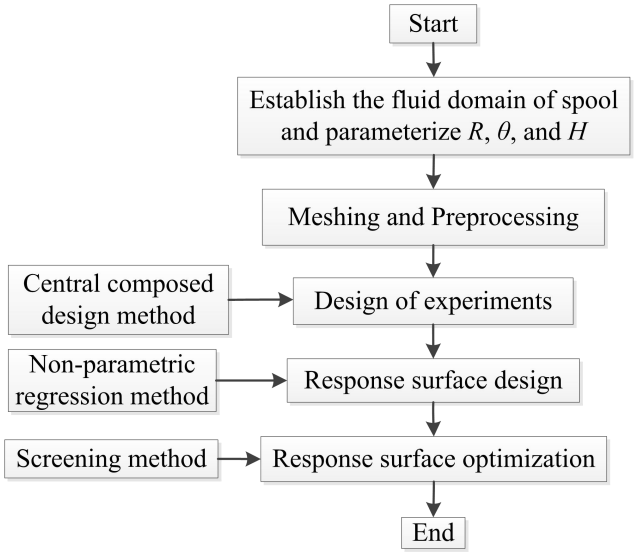

FIGURE 13. Optimization design flowchart.

First, the fluid model of the spool turbine bucket profile is established using CAD software, and R, θ, and H are parameterized. Second, the grid meshing and preprocessing are conducted according to the spool CFD modeling method in Section IV, in which the velocity of the inlet domain is 2.25 m/s, the throttle opening of the motion domain is 0.05 mm, and the steady flow force F_s is defined as the output parameter. Finally, the experiments are designed.

A. DESIGN OF EXPERIMENTS

Design of experiments is to collect the design parameter samples according to the number of input parameters, calculate the response results of each sample, and construct the response surface or response curve of the design space by using quadratic interpolation. The design types of experiment include central composed design (CCD), optimal space-filling design and Box-Behnken design. As the CCD can be valued to the maximum and minimum values of the design parameter range, this study selects the CCD for sample generation. Fifteen samples are selected in the three-dimensional space, which include one central point, six axis points, and eight diagonal points, respectively [29]. The samples and simulation results of the steady flow force F_{sim} are shown in Table 1.

B. RESPONSE SURFACE DESIGN

The response surface model is generated by non-parametric regression method using the results of experimental designs. The single parameter response surface models of steady flow force about R, θ, and H are generated as shown in Figs. 14-16, respectively. As shown in Fig. 14, the steady flow force of the spool slowly increases with R when $R < 1.5$ mm and rapidly decreases with the increase in R when $R > 1.5$ mm. Fig. 15 shows that the steady flow force increases with θ when $\theta > 65°$ and decreases with the increase in θ when $\theta < 65°$.

TABLE 1. Samples and simulation results.

Numbers	H/mm	R/mm	θ/°	F_{sim}/N
1	1.75	2	56.25	7.0423
2	0	2	56.25	6.9791
3	3.5	2	56.25	7.1457
4	1.75	0.5	56.25	7.0185
5	1.75	3.5	56.25	6.6663
6	1.75	2	22.5	6.875
7	1.75	2	90	6.9633
8	0.32719	0.78045	28.81	7.0582
9	3.1728	0.78045	28.81	6.6289
10	0.32719	3.2196	28.81	6.8571
11	3.1728	3.2196	28.81	6.5571
12	0.32719	0.78045	83.69	7.0028
13	3.1728	0.78045	83.69	7.2765
14	0.32719	3.2196	83.69	7.3086
15	3.1728	3.2196	83.69	6.7336

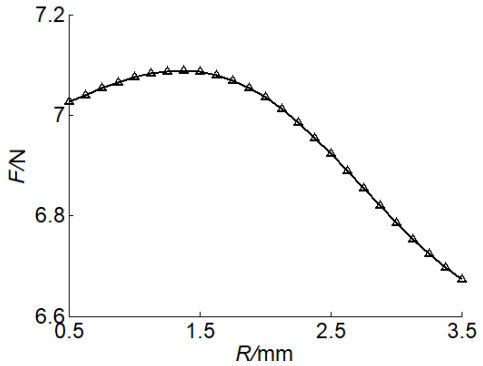

FIGURE 14. Single-parameter response surface of R.

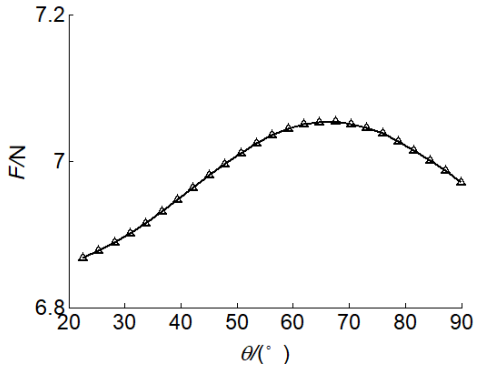

FIGURE 15. Single-parameter response surface of θ.

Fig. 16 shows that the steady flow force increases with H. Fig. 17 shows the local sensitivity of R, θ, and H to steady flow force. R is evidently the most sensitive factor of the steady flow force, followed by θ, and H is the least sensitive factor.

To verify whether the designed response surface model calculates the steady flow force of the spool accurately, another five samples are randomly generated to compare the steady flow force F_{sim} calculated by the CFD model with the steady flow force F_{cal} calculated by the designed response surface. The samples and the results are shown in Table 2. Finally, the error determination coefficient R_e^2 is used to evaluate the

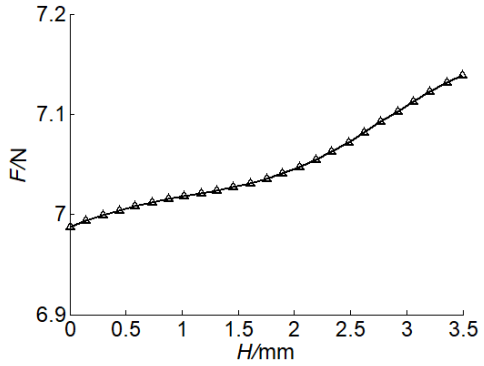

FIGURE 16. Single-parameter response surface of H.

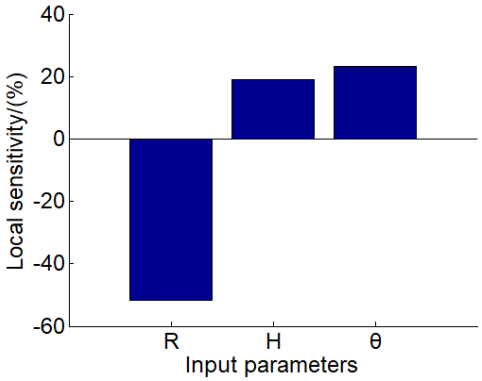

FIGURE 17. Local sensitivity of input parameters.

TABLE 2. Verification of response surface.

Numbers	R/mm	H/mm	θ/°	F_{sim}/N	F_{cal}/N
1	3.4762	2.0032	86.467	7.1316	7.1094
2	1.7822	3.4749	23.864	6.5845	6.6222
3	1.7582	0.69705	89.319	7.0145	7.0699
4	3.4234	0.62757	56.508	7.0569	7.0705
5	1.7333	3.4538	87.672	6.9269	6.9107

quality of the designed response surface [30].

$$R_e^2 = 1 - \frac{\sum_{i=1}^{N} [y_{\text{rsm}}(i) - y(i)]^2}{\sum_{i=1}^{N} [y(i) - \bar{y}]^2}, \tag{8}$$

where $y_{\text{rsm}}(i)$ is the value of the sample calculated by the response surface, $y(i)$ is the value of the sample calculated by the CFD model, $\bar{y}$ is the average value of the sample calculated by the CFD model, and N is the number of samples. When R_e^2 is close to 1, the agreement between the response surface model and the CFD model of spool is good.

The error determinant coefficient R_e^2 is equal to 0.9671, which is calculated by Formula (8). Thus, the designed response surface model can approximate the CFD model of the spool well.

C. RESPONSE SURFACE OPTIMIZATION

Response surface optimization is to obtain the optimal parameter values of R, θ, and H to make F_s the smallest.

TABLE 3. Comparison of the steady flow force of the optimized valve with the original valve.

	R/mm	θ/°	H/mm	F_s
Original spool	0.5	90°	0	6.9827
Optimized spool	3.4	25°	3.2	6.5413

FIGURE 18. Original and optimized spools.

Limited by manufacturing, axial and radial dimensions of the spool groove, R is valued between 0.5mm and 3.5mm, θ is valued between 22.5° and 90°, and H is valued between 0 and 3.5mm. Therefore, the mathematical model of the parameter optimization for the spool turbine bucket can be summarized as follows [30]:

$$\min \ (F_s) \quad s.t. \begin{cases} 0.5\text{mm} \le R \le 3.5\text{mm} \\ 22.5° \le \theta \le 90° \\ 0 \le H \le 3.5\text{mm}. \end{cases} \tag{9}$$

ANSYS Workbench offers different goal-driven optimization methods. The screening method is selected to calculate the optimal solution. Moreover, the optimization result of the design parameters is rounded to facilitate manufacturing and detection. The optimal parameters of the turbine bucket profile eventually become $R = 3.4$ mm, $\theta = 25°$, and $H = 3.2$ mm. The steady flow forces of the original and the optimized spools are calculated through the designed response surface, as shown in Table 3. The steady flow force of the optimized spool can be reduced by 6.3% compared with that of the original spool.

As the CFD simulation has a convergence error, the smaller the error is, the more accurate the optimal solution would be, however, the computing speed of the CFD simulation would be slowly too. Therefore, the compensation effect of the optimal solution on steady flow force needs to be verified by experiments to verify the rationality of the convergence criteria setting during the CFD simulation further.

VI. TEST VERIFICATION

The optimized and the original spools are manufactured to verify the steady flow force compensation effect of the optimized spool (Fig. 18).

The anti-flow impact performances of the optimized and original spools are compared through the test bench in Section IV. The specific experimental steps of anti-flow impact test are as follows.

First, the overflow of the optimized spool (or the original spool) is maintained at 8 L/min, and the original pressure in the main spool chamber remains at 0.5 MPa by adjusting the driving current of the proportional solenoid valve.

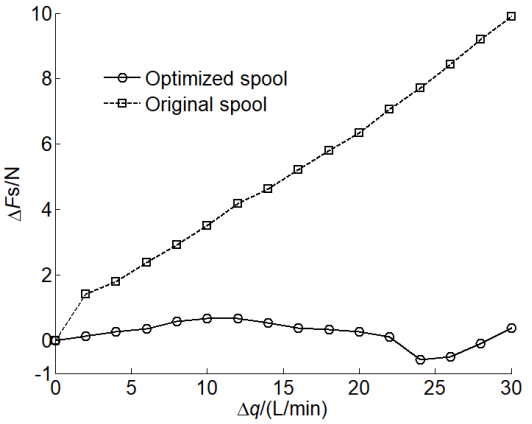

FIGURE 19. Original pressure is 0.5 MPa.

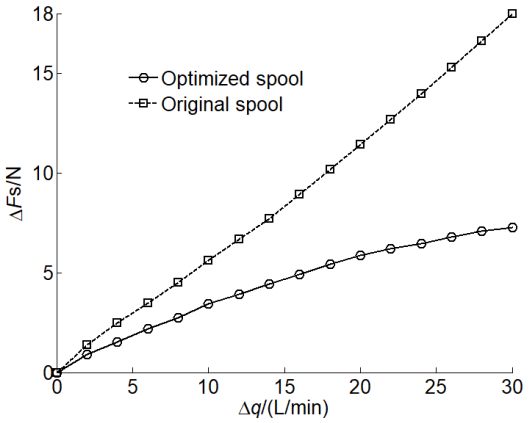

FIGURE 20. Original pressure is 2 MPa.

Second, the overflow of the spool increases to 38 L/min at an increment of 2 L/min by adjusting the speed of the driving motor. The pressure in the main chamber of the spool p is measured by pressure sensor 7 at different overflow conditions.

Finally, the steady flow force increment of the spool at different overflow conditions can be calculated by Formula (10), and the relationship between the steady flow force increment ΔF_s and the flow increment Δq can be plotted, as shown in Fig. 19.

$$\Delta F_s = (p - p_0)\, A_{\text{feedback}}, \tag{10}$$

where p_0 is the original pressure in the main chamber of the spool.

By analogy, the relationships between the steady flow force increment and the flow increment are measured when the original pressure of the optimized and original spools are 2 MPa and 4 MPa, as shown in Figs. 20 and 21, respectively.

Figs. 19–21 show that the steady flow force increment of the optimized spool is evidently smaller than that of the original spool with the increase in overflow under different original pressures. When the overflow increment is 30 L/min, the steady flow force of the optimized spool can be reduced by approximately 10 N compared with that of the original spool. The steady flow force increment is approximately linear with

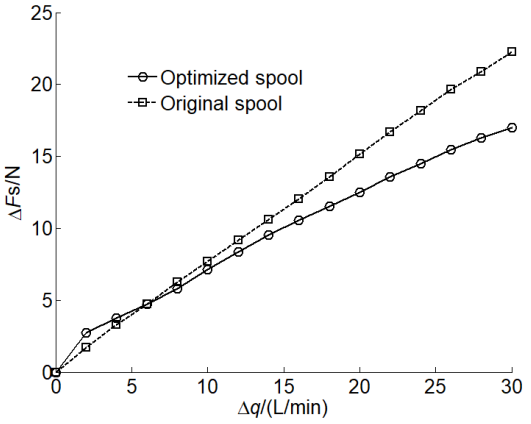

FIGURE 21. Original pressure is 4 MPa.

TABLE 4. Flow impact coefficient.

Pressure (MPa)	Optimized spool	Original spool
0.5	−0.0151	0.3084
2	0.2407	0.5892
4	0.5436	0.7418

the overflow increment regardless of the original or optimized spool. However, the steady flow force increment of the optimized spool in Fig. 19 fluctuates near the zero axis with the increase of flow. It is mainly because the optimized spool can completely compensate the steady flow force and the measurement error of the pressure sensor is bigger compared to the main chamber pressure when it is small, resulting in the main chamber pressure fluctuates near 0.5MPa.

To illustrate quantitatively the effect of the optimized spool on steady flow force compensation, the flow impact coefficient β is defined as the steady flow force increment at per unit overflow increment. The more β is greater than 0, indicating that the more steady flow force the spool compensates. The more β is less than 0, indicating that the more steady flow force the spool overcompensates. When β equals 0, it indicates that the spool can fully compensate steady flow force.

$$\beta = \frac{\Delta F_s}{\Delta q} \tag{11}$$

The first-order least square method is used to fit the flow impact coefficients of the original and optimized spools under different original pressures, as shown in Table 4. With the increase of original pressure, the flow impact coefficient of the original and optimized spools gradually increases; thus, the steady flow force compensation capacity of the spools worsens with the increase in pressure. However, the flow impact coefficient of the optimized spool is evidently smaller than that of the original spool under different original pressures. When the original pressure is 0.5MPa, the flow impact coefficient of the optimized spool is a negative which is close to 0, indicating that the optimized spool can fully compensate steady flow force. The reason that the flow impact coefficient is a negative is as same as the curve of the optimized spool in Fig. 19 fluctuates near the zero axis. When the original

pressure is 2MPa, the flow impact coefficient of the optimized spool is reduced by up to 59.15% compared to the original spool. When the original pressure is 4MPa, the flow impact coefficient of the optimized spool is reduced by up to 26.72% compared to the original spool. Hence, the steady flow force compensation capacity of the optimized spool is clearly better than that of the original spool. And with the working pressure decreasing, the steady flow force compensation of the optimized spool is becoming more and more obvious.

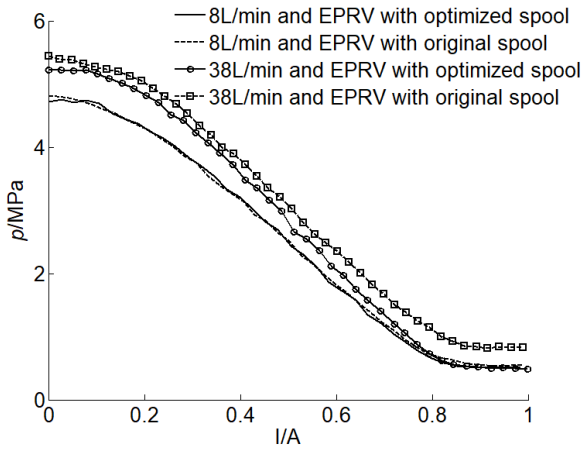

FIGURE 22. Pressure–current characteristic curve of EPRV.

To verify the effect of the optimized spool on the pressure control accuracy of the EPRV, the pressure–current curve of the EPRV with optimized and original spools are compared by adjusting the driving current from 0 A to 1 A linearly under an overflow of 8 L/min and 38 L/min (Fig. 22). When the overflow is 8 L/min, the pressure–current curve of the EPRV with optimized spool coincides with the EPRV with original spool well; thus, the steady flow force does not affect the pressure–current characteristics of the EPRV. When the overflow changes to 38 L/min, the pressure rise offset of the EPRV with optimized spool is evidently smaller than that of the EPRV with original spool; thus, the optimized spool can clearly improve the control accuracy of the EPRV. The pressure rise offset caused by the flow step of the EPRV with optimized spool evidently decreases with the working pressure. It means that the optimized spool can improve more control accuracy of the EPRV as the working pressure decreasing.

VII. CONCLUSION

Given that the overflow extensively changes, the steady flow force of the spool will change and affect the working pressure of the relief valve, thereby influencing the pressure control accuracy of the EPRV eventually. This study focus on how to reduce the steady flow force maximally through designing the turbine bucket profile in the spool groove. The following conclusions can be drawn.

(1) The absolute error value of test and simulation of the spool CFD model that considers fitting clearance is smaller than 6.51%. Therefore, for the low power spool, the effect of fitting clearance on steady flow force calculation cannot be ignored when the spool CFD model is established.

(2) Among the three design parameters of turbine bucket profile, the radius of the arc groove, the conical angle, and the conical height, the steady flow force increases initially and then decreases with the increase in the radius of the arc groove, decreases initially and then increases with the conical angle, decreases gradually with the increase in the conical height.

(3) When the working pressure are 0.5MPa, 2MPa and 4MPa, the flow impact coefficients of the optimized spool can be reduced by 100%, 59.15% and 26.72% respectively compared with the original spool. It means that the optimized spool can obviously compensate the steady flow force. Thus, the CFD model of spool and the response surface model of steady flow force have high accuracy to obtain the optimal solution of turbine bucket profile.

(4) The optimized spool can clearly improve the pressure control accuracy of the EPRV. The influence of flow step on the pressure control accuracy of the EPRV with optimized spool obviously decreases with the working pressure.

REFERENCES

[1] J. Xuan and S. Wang, "Development of hydraulically driven fatigue testing machine for insulators," *IEEE Access*, vol. 6, pp. 980–988, 2018.
[2] J. Li, M. Ding, W. Yong, and C. Li, "Evaluation and optimization of the nonlinear flow controllability of switch valve in vehicle electro-hydraulic brake system," *IEEE Access*, vol. 6, pp. 31281–31293, 2018.
[3] S. M. Savaresi, M. Tanelli, F. L. Taroni, F. Previdi, and S. Bittanti, "Analysis and design of an automatic motion inverter," *IEEE/ASME Trans. Mechatronics*, vol. 11, no. 3, pp. 346–357, Jun. 2006.
[4] D. Qu, L. Wei, L. Yunfeng, F. Bing, Z. Yunshan, Z. Feitie, "Simulation and experimental study on the pump efficiency improvement of continuously variable transmission," *Mech. Mach. Theory*, vol. 131, pp. 137–151, Jan. 2019.
[5] E. Lisowski, W. Czyżycki, and J. Rajda, "Three dimensional CFD analysis and experimental test of flow force acting on the spool of solenoid operated directional control valve," *Energy Convers. Manage.*, vol. 70, pp. 220–229, Jun. 2013.
[6] R. Amirante, G. Dal Vescovo, and A. Lippolis, "Flow forces analysis of an open center hydraulic directional control valve sliding spool," *Energy Convers. Manage.*, vol. 47, no. 1, pp. 114–131, Jan. 2006.
[7] H. Xie, L. Tan, J. Liu, H. Chen, and H. Yang, "Numerical and experimental investigation on opening direction steady axial flow force compensation of converged flow cartridge proportional valve," *Flow Meas. Instrum.*, vol. 62, pp. 123–134, Aug. 2018.
[8] G. Altare, M. Rundo, and M. Olivetti, "3D dynamic simulation of a flow force compensated pressure relief valve," in *Proc. Int. Mech. Eng. Congr. Expo.*, Phoenix, AZ, USA, Nov. 2016, pp. 11–17.
[9] R. Finesso and M. Rundo, "Numerical and experimental investigation on a conical poppet relief valve with flow force compensation," *Int. J. Fluid Power*, vol. 18, no. 2, pp. 111–112, Feb. 2017.
[10] J. F. Blackburn, Ed. *Fluid Power Control*. Cambridge, MA, USA: MIT Press, 1969.
[11] H. Merritt, H. E. Merritt, and H. E. Merritt, *Hydraulic Control Systems*. Hoboken, NJ, USA: Wiley, 1967.
[12] J. Lugowski. (2013). "Steady-state flow-force compensation in a hydraulic spool valve." [Online]. Available: https://arxiv.org/abs/1312.1310
[13] M. Borghi, M. Milani, and R. Paoluzzi, "Stationary axial flow force analysis on compensated spool valves," *Int. J. Fluid Power*, vol. 1, no. 1, pp. 17–25, Jan. 2000.

[14] N. Z. Aung, P. Jinghui, and L. Songjing, "Reducing the steady flow force acting on the spool by using a simple jet-guiding groove," in *Proc. Int. Conf. Fluid Power Mechatron. (FPM)*, Aug. 2015, pp. 289–294.
[15] M. Simic and N. Herakovic, "Reduction of the flow forces in a small hydraulic seat valve as alternative approach to improve the valve characteristics," *Energy Convers. Manage.*, vol. 89, pp. 708–718, Jan. 2015.
[16] R. Amirante, E. Distaso, and P. Tamburrano, "Sliding spool design for reducing the actuation forces in direct operated proportional directional valves: Experimental validation," *Energy Convers. Manage.*, vol. 119, pp. 399–410, Jul. 2016.
[17] R. Amirante, P. G. Moscatelli, and L. A. Catalano, "Evaluation of the flow forces on a direct (single stage) proportional valve by means of a computational fluid dynamic analysis," *Energy Convers. Manage.*, vol. 48, no. 3, pp. 942–953, Mar. 2007.
[18] R. Amirante, L. A. Catalano, C. Poloni, and P. Tamburrano, "Fluid-dynamic design optimization of hydraulic proportional directional valves," *Eng. Optim.*, vol. 46, no. 10, pp. 1295–1314, Jul. 2014.
[19] R. Amirante, C. L. Andrea, and P. Tamburrano, "The importance of a full 3D fluid dynamic analysis to evaluate the flow forces in a hydraulic directional proportional valve," *Eng. Comput.*, vol. 31, no. 5, pp. 898–922, Jul. 2014.
[20] Q. Yuan and P. Y. Li, "Using steady flow force for unstable valve design: Modeling and experiments," *J. Dyn. Syst., Meas., Control*, vol. 127, no. 3, pp. 451–462, Sep. 2005.
[21] Q. Chan, L. Zhenyu, P. Xiang, and T. Jianrong, "A non-ideal geometry based prediction approach of fitting performance and leakage characteristic of precision couplings," *IEEE Access*, vol. 6, pp. 58204–58212, 2018.
[22] J. Deng, X.-M. Shao, X. Fu, and Y. Zhenga, "Evaluation of the viscous heating induced jam fault of valve spool by fluid–structure coupled simulations," *Energy Convers. Manage.*, vol. 50, no. 4, pp. 947–954, Apr. 2009.
[23] C. Qianpeng, J. Hong, Z. Yi, and Y. Xubo, "Proposal for optimization of spool valve flow force based on the MATLAB-AMESim-FLUENT joint simulation method," *IEEE Access*, vol. 6, pp. 33148–33158, 2018.
[24] I. Okhotnikov, S. Noroozi, P. Sewell, and P. Godfrey, "Evaluation of steady flow torques and pressure losses in a rotary flow control valve by means of computational fluid dynamics," *Int. J. Heat Fluid Flow*, vol. 64, pp. 89–102, Apr. 2017.
[25] G. Del Vescovo and A. Lippolis, "Three-dimensional analysis of flow forces on directional control valves," *Int. J. Fluid Power*, vol. 4, no. 2, pp. 15–24, Jun. 2003.
[26] J. Tao, X. Mingjie, and W. Anlin, "Applicability analysis of slide valve in 3D trainsient flow field analysis of sliding method method," *Tongji Univ.*, vol. 43, no. 10, pp. 1575–1581, 2015.
[27] G. R. Wang, F. Chu, S. Y. Tao, L. Jiang, and H. Zhu, "Optimization design for throttle valve of managed pressure drilling based on CFD erosion simulation and response surface methodology," *Wear*, vols. 338–339, pp. 114–121, Sep. 2015.
[28] C. Zhang and G. Li, "Optimization of a direct-acting pressure regulator for irrigation systems based on CFD simulation and response surface methodology," *Irrigation Sci.*, vol. 35, no. 5, pp. 383–395, Sep. 2017.
[29] M. A. Bezerra, R. E. Santelli, E. P. Oliveira, L. S. Villar, and L. A. Escaleira, "Response surface methodology (RSM) as a tool for optimization in analytical chemistry," *Talanta*, vol. 76, no. 5, pp. 965–977, Sep. 2008.
[30] X. F. Wu, W. Gan, C. Liu, and X. Wang, "Robust Design of Hydraulic Slide Valve Internal Structure," *China Mech. Eng.*, vol. 26, no. 15, pp. 2030–2035, Aug. 2015.

DAOHAI QU was born in Shiyan, Hubei, China, in 1989. He received the B.S. degree in vehicle engineering from the Hubei University of Automotive Technology, Shiyan, in 2012, and the M.S. degree in vehicle engineering from Hunan University, Changsha, China, in 2014, where he is currently pursuing the Ph.D. degree in mechanical engineering.

Since 2014, he has been a Hydraulic Engineer with Hunan Rongda Vehicle Transmission Co., Ltd., where he is mainly responsible for designing and testing the hydraulic systems of hybird vehicle transmission systems. His current research interest includes hydraulic transmission and control.

YUNSHAN ZHOU was born in Qidong, Hengyang, China, in 1957.He received the B.S., M.S., and Ph.D. degrees in vehicle engineering from Jilin University, Jilin, China, in 1984, 1987 and 1990, respectively.

From 1984 to 2003, he was an Assistant Professor and a Professor with the College of Automotive Engineering, Jilin University. From 1999 to 2002, he was a Visiting Scholar with the University of Illinois at Urbana–Champaign. He holds the membership of China gear manufacturing industry and is the Technical Director of Hunan Rongda Vehicle Transmission Co., Ltd. He has authored three books, more than 40 articles, and more than 30 inventions. Since 2004, he has been a Professor with the College of Mechanical and Vehicle Engineering, Hunan University, Changsha, China. His research interests include continuously variable transmission technology, hydraulic drive control, electronic control suspension, and hybrid transmissions. He is an Editor of *Automobile Technology*, the *Transactions of the Chinese Society of Agricultural Machinery*, and the *Journal of Beijing Institute of Technology*.

YUNFENG LIU was born in Junshanpu, Changde, China, in 1989. He received the B.S. degree in thermal energy and power engineering and the M.S. degree in power engineering from Hunan University, Changsha, China, in 2011 and 2014, respectively. He is currently pursuing the Ph.D. degree in mechanical engineering with Hunan University, Changsha.

Since 2014, he has been a Calibration Engineer with Hunan Rongda Vehicle Transmission Co., Ltd., where his main responsibilities include hybrid transmission and motor calibrating work, and hybrid power battery debugging work. His research interests include hybrid transmission control, electric motor control, and battery management system control.

WEI LUO was born in Anlu, Hubei, China, in 1986. He received the B.S. degree in mechanical engineering and automation and the M.S. degree in mechanical and electronic engineering from the Wuhan University of Science and Technology, Wuhan, China, in 2009 and 2012, respectively. He is currently pursuing the Ph.D. degree in mechanical engineering with Hunan University, Changsha, China.

Since 2012, he has been the Hydraulic Chief Engineer with Hunan Rongda Vehicle Transmission Co., Ltd., where his main responsibilities include the development and validation of hydraulic systems in continuously variable transmission, hybrid power, and pure electric power transmission. His research interests include the development of hydraulic and electronic control systems, hybrid power, and pure electric power transmission systems.

FEITIE ZHANG was born in Longhui, Shaoyang, China, in 1978. He received the B.S., M.S., and Ph.D. degrees in vehicle engineering from Hunan University, Changsha, China, in 2000, 2004, and 2008, respectively.

His research interests include automatic transmission control systems, new energy vehicle powertrain control systems (motor controller), and intelligent control systems of intelligent vehicle based on image recognition technology. From 2004 to 2009, he was a Software Engineer with Hunan Rongda Vehicle Transmission Co., Ltd., where he is mainly responsible for continuously variable transmission control unit software development work. Since 2010, he has been an Assistant Professor of mechanical engineering with Hunan University. From 2013 to 2014, he was a Visiting Scholar with the Power Assembly Laboratory, University of Michigan.